THE ASTROPHYSICAL JOURNAL, 448:164–178, 1995 July 20

MULTIFREQUENCY RADIO STUDIES OF G359.1−00.2

ANDREW D. GRAY
School of Physics, University of Sydney, NSW 2006, Australia; and Dominion Radio and Astrophysical Observatory, Herzberg Institute of Astrophysics, National Research Council Canada, Box 248, Penticton, BC, V2A 6K3, Canada

JENNIFER NICHOLLS
Research Centre for Theoretical Astrophysics, School of Physics, University of Sydney, NSW 2006, Australia

RON D. EKERS
Australia Telescope National Facility, PO Box 76, Epping, NSW 2121, Australia

AND

LAWRENCE E. CRAM
School of Physics, University of Sydney, NSW 2006, Australia
Received 1994 November 3; accepted 1995 January 23

ABSTRACT

The Molonglo Observatory Synthesis Telescope, the Australia Telescope Compact Array, and the Very Large Array have been used to carry out imaging and polarimetry experiments on the unusual Galactic center filamentary object G359.1−00.2, also known as "the Snake." The observations were carried out at 843, 1446, 4790, 5840, and 8640 MHz, with resolutions as fine as 2″. The images reveal intricate internal structure in the object and physical properties similar to previously recognized filamentary features in the region. Several models of the source are discussed, with some form of electrodynamic activity being favored at present. It is not possible, however, to rule out all other models discussed—a jet or ejectum from a supernova event, a star wake or trail, a shock front, a phenomenon related to a cosmic string or the nearby "Great Annihilator," 1E1740.7−2942, a morphologically unusual supernova remnant—conclusively. Several models do predict observable changes in the source on timescales of years, so further observations will help clarify this issue.

A fractional linear polarization as high as ∼50% was found for part of the Snake, although some regions of the source are completely depolarized. The frequency dependence of the observed polarization properties suggests a model of the source as a twisted ribbon embedded in a thermal medium giving rise to an external rotation measure of at least 5500 rad m^{-2}, with strong depolarization due to an internal Faraday depth of up to 1400 rad m^{-2}. The derived properties of the thermal medium in this model require a thermal electron density of 10 cm^{-3} with a line-of-sight magnetic field strength of 7 μG along a path of length ∼100 pc. These parameters are consistent with material in a nuclear disk in the Galactic center.

Subject headings: Galaxy: center — ISM: individual (G359.1−00.2) — ISM: structure — polarization — radio continuum: ISM

1. INTRODUCTION

The Galactic center region has been the subject of intense study at radio wavelengths since being identified with the nuclear region of our Galaxy (see, for example, McGee & Bolton 1954). Some reviews of the many discoveries over the decades have been published by Oort (1977), Brown & Liszt (1984), Genzel & Townes (1987), Backer (1987), Morris (1989), and Blitz et al. (1993). Of particular interest to the work presented here are the detailed, interferometric, radio continuum observations of the Galactic center region made in the early 1980s, revealing previously unimagined fine detail in and around the nuclear complex, Sgr A (Yusef-Zadeh, Morris, & Chance 1984). In particular, long, narrow, filaments were found, with others soon identified in nearby regions (Morris & Yusef-Zadeh 1985; Bally & Yusef-Zadeh 1989; Bally, Yusef-Zadeh, & Hollis 1989). All are characterized by long, thin structure, with spectra ranging from flat to typical nonthermal power laws of index $\alpha \simeq -0.5$. Several are known to display significant polarization. The most recently discovered example of this class of object is G359.1−00.2—also known as "the Snake" (see Fig. 1)—revealed during the 843 MHz ($\lambda = 35.6$ cm) Galactic center Survey completed using the Molonglo Observatory Synthesis Telescope (hereafter MOST: Mills 1981; Robertson 1991). Full details of the survey, including survey images, are published elsewhere (Gray 1994a), with detailed discussions of previously known and newly discovered supernova remnants—including their distribution and relationship to known pulsars—being found in Gray (1994b, c, d).

Subsequent to its discovery with MOST, the Snake was observed at higher frequencies and resolutions using the Very Large Array[1] (VLA; see Napier, Thompson, & Ekers 1983) and the Australia Telescope Compact Array (hereafter ATCA; see Australia Telescope 1992). Initial results of these studies (Gray et al. 1991) showed that the object has several interesting properties even among similar filamentary objects in the region, including a unique "kinked" structure. This paper presents further details of these follow-up studies, including improved total intensity images and new polarimetry results

[1] The VLA is a facility of the National Radio Astronomy Observatory, which is operated by Associated Universities, Inc., under contract with the National Science Foundation.

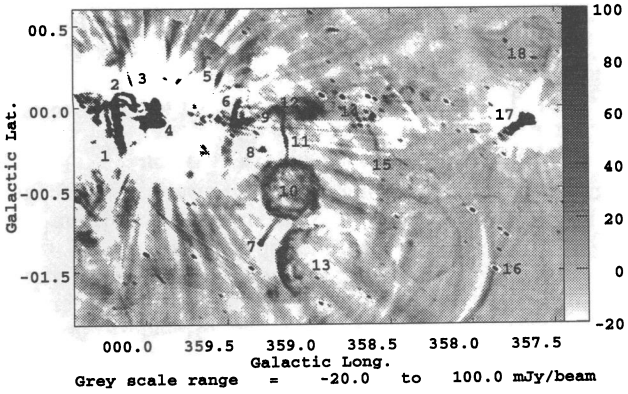

FIG. 1.—A montage of MOST 843 MHz images showing the region around the Snake (object 11). The numbered sources are listed in Table 2, and many feature in the discussions in the text.

obtained from data collected with the VLA at 1446 MHz and the ATCA at 4790, 5840, and 8640 MHz, together with interpretation and discussion of these results. Section 2 details the data acquisition and reduction of these observations. The Stokes *I* results and the derived properties of the Snake are discussed in § 3, and the polarimetry results and their implications for the structure of the Snake and the surrounding interstellar medium are discussed in § 4.

2. DATA ACQUISITION AND REDUCTION

2.1. *VLA* 1446 MHz *Observation*

A field centered at $17^h44^m22^s.00$, $-29°46'00''.0$ (J2000.0) was observed on 1990 October 11 using the VLA in the CnB hybrid configuration to give a nearly circular beam. Data were accumulated for 6 hr in continuum mode at 1446.15 MHz ($\lambda = 20.7$ cm) and 1496.15 MHz ($\lambda = 20.0$ cm) simultaneously. The IF bandwidth at each frequency was 12.5 MHz, chosen to maximize sensitivity but limit bandwidth smearing effects to ~5% at the half-power radius of the primary beam (see Bridle & Schwab 1989). Both co-polar (*RR*, *LL*) and cross-polar (*RL*, *LR*) complex correlations of the circularly polarized signals were recorded for each antenna pair at both frequencies with a 30 s sampling interval. Flux density was calibrated against 3C 48 (B0134+329), assumed to be 15.83 and 15.42 Jy at the respective IF frequencies. The phase reference calibrator was B1748−253, which has a flux density of ~1 Jy at 1.4 GHz and lies only 4° from the Snake.

The data were reduced following standard AIPS procedures (see Greisen & Junor 1990), producing images of Stokes *I*, *Q*, *U*, and *V* from frequency-averaged data. No significant signal was detected in the *Q*, *U*, or *V* images, but in view of the large rotation measures in this region (see, for example, Tsuboi et al. 1986; Yusef-Zadeh & Morris 1987b) this is not necessarily evidence for the source itself being unpolarized. The *I* image was self-calibrated and a CLEAN component model of Sgr A—0°.9 away, or nearly 4 times the half-power radius of the primary beam—was subtracted from the visibility data to reduce sidelobes. This was not entirely successful since at this distance from the field center the amplitude of Sgr A was modulated by its relative motion through the noncircularly symmetric sidelobe patterns of the primary beam. In addition to Sgr A, a ~400 mJy unresolved source at $17^h42^m44^s.0$, $-29°49'14''$ (J2000.0) was also subtracted. This object lies at the edge of the Sgr E complex, has a nonthermal spectrum, and is probably a background object (see Gray et al. 1993). The final *I* image was deconvolved and restored with a Gaussian beam of size $15''.8 \times 11''.4$ P.A. 52°.8 (see Fig. 2). The rms noise achieved was 0.2 mJy beam^{-1} (confusion and dynamic range limited).

2.2. *ATCA* 4790, 5840, *and* 8640 MHz *Observations*

ATCA observations of the Snake were made in 1990 (June, July, November), 1991 (February, May September), and 1993 (April). All observations were for 12 hours duration to ensure full hour angle coverage from the ATCA's east-west baseline, and used the 32 channel, 128 MHz bandwidth continuum mode. The sampling period was generally 10 s sampling interval, although some observations used 15 or 20 s. All observations were at 4790 MHz ($\lambda = 6.26$ cm) except for 1993 April, which was at simultaneous frequencies 5840 and 8640 MHz ($\lambda = 5.13$ and 3.47 cm). Owing to on-going instrumental development, observations until 1991 May recorded only co-polar (*XX*, *YY*) complex correlations of the linearly polarized signals from five antennas, while the 1991 September and 1993 April observations recorded both co-polar and cross-polar (*XY*, *YX*) complex correlations for six antennas.

Array configurations with nominal maximum baselines of 1.5 km (24 kλ at 4790 MHz) or 3.0 km (48 kλ) were used, which included some baselines in the range 3.0–6.0 km for 1991 September and 1993 April when the sixth antenna was available. The 4790 MHz data were collected on four pointing centers ("N," "C," "S," and "S 2" in Table 1) arranged along the long axis of the Snake and separated by the half-power radius of the primary beam (5′) to allow the use of mosaicking techniques for wide-field imaging (Cornwell 1989). Owing to the sparse *u-v* coverage afforded by a single ATCA configuration, each pointing center was observed using three ("N" and "S2") or five ("C" and "S") different configurations. The higher frequency data from 1993 April used a single configuration on pointing center "C2" (see Table 1).

Flux density was calibrated against B1934−638. Note that the spectrum of this object as used for calibration of ATCA data has been revised recently; at the time of the preparation of the gray-scale figures presented in this paper the adopted flux densities were 6.35 Jy at 4790 MHz, 4.82 Jy at 5840 MHz, and

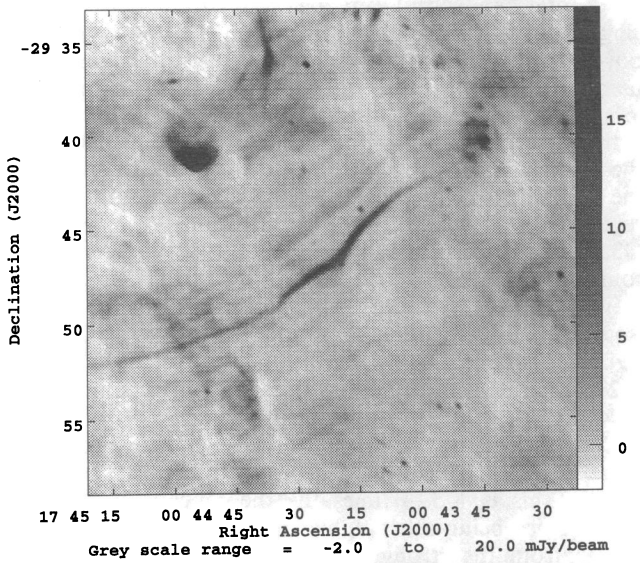

FIG. 2.—The 1446 MHz VLA image of the Snake. A single 6 hour observation was used to make this image, which has a resolution of $15''.8 \times 11''.4$ P.A. 52°.8. Note that the apparent feature to the north of and parallel to the Snake is a residual sidelobe.

TABLE 1

POINTING POSITIONS USED IN ATCA OBSERVATIONS OF THE SNAKE

Label	R.A. (J2000.0)	Decl. (J2000.0)
N.....	$17^h44^m03^s.815$	$-29°42'54''.93$
C.....	17 44 22.000	−29 46 00.00
C2.....	17 44 22.000	−29 46 30.00
S	17 44 35.023	−20 48 52.42
S2	17 44 54.000	−29 51 30.00

NOTE.—The position labeled "C2" was used for 5840/8640 MHz polarimetric observations; the other four were used for the 4790 MHz mosaicking observations.

2.59 Jy at 8640 MHz. The flux densities now recommended are 5.84 Jy at 4790 MHz (92% of its former value), 4.62 Jy at 5840 MHz (96%), and 2.84 Jy at 8640 MHz (110%). In this paper, corrections based on these new values have been applied *only* to data used in numerical discussions (i.e., the figures remain unchanged).

For polarimetric calibration, the polarized source 3C 138 (B0518+165) was also observed during 1991 September and 1993 April. The phase reference calibrator used at 4790 MHz was B1748−253 (0.52 Jy), while B1741−312, which has a flatter spectrum, was used at 5840 and 8640 MHz (0.43 Jy and 0.40 Jy, respectively). These were observed briefly at half hourly intervals throughout the observations, and since they are unpolarized were also used to determine instrumental polarization. For Stokes *I* imaging, the data were reduced in AIPS following the same procedures used for the VLA data reduction (Killeen 1992). Since AIPS assumes that the data is recorded by circularly polarized feeds; however, it cannot treat the linear polarization data recorded by the ATCA correctly, and polarimetric calibration was completed in the MIRIAD package (Sault & Killeen 1992).

2.2.1. 4790 MHz *Wide-Field Stokes I Mosaic*

A wide-field image was prepared from 4790 MHz data on pointing centers N, C, S, and S2, using baselines ≤ 24 kλ. In making images of the four pointing centers, channels 5–29 (100 MHz total bandwidth) were averaged together without inducing bandwidth smearing effects greater than $\sim 5\%$ at the half-power radius of the primary beam. An MEM algorithm was used (AIPS task VTESS; see Cornwell 1989) to carry out a joint deconvolution to "mosaic" the images together. To assist with convergence, sources not believed to be associated with the Snake were first removed by CLEANing without restoring the subtracted components. The sources removed were H II region G359.28−0.26 (FIR 27; Odenwald 1989); H II region G359.186−0.026 (Caswell & Haynes 1987); a 12 mJy point source at $17^h44^m52^s.22$, $-29°53'32''.3$ (J2000.0) (source 1); an 11 mJy point source at $17^h44^m28^s.65$, $-29°41'53''.2$ (J2000.0) (source 2); a 7 mJy point source at $17^h44^m14^s.85$, $-29°43'57''.1$ (J2000.0) (source 3); a 6 mJy point source at $17^h43^m53^s.71$, $-29°42'56''.5$ (J2000.0) (source 4); and a 4 mJy point source at $17^h44^m03^s.74$, $-29°39'13''.9$ (J2000.0) (source 5).

Convergence was achieved for an rms noise of 80 μJy beam^{-1} on each field, with a beam of size $13''.7 \times 7''.2$ P.A. $-0°.8$. This is $\sim$3–4 times the theoretical noise, with the excess noise being attributable to dynamic range limitations arising from the strong sources in the region. Finally, the mosaiced image was masked where the primary-beam–boosted noise exceeded 275 μJy beam^{-1} (or 5 times the minimum rms noise in the mosaic, which is lower than the rms noise on the individual fields owing to field overlap). A gray-scale representation of the mosaic is shown in Figure 3. Because the subtracted sources are not of interest to this study, they have not been restored to the final image, although their positions are marked in Figure 3.

2.2.2. *High-Resolution Stokes I Mosaic*

Images of pointing centers C and S were also prepared without the restriction on the maximum baseline imposed above, thereby including baselines up to 6.0 km (96 kλ). Channels 5–29 were again used, but the increase in spatial resolution made it necessary to consider the frequency of each channel when gridding the *u-v* data to avoid bandwidth smearing. Unfortunately, it was discovered that a sampler problem in the sixth antenna, which is present in all baselines greater than 3.0 km, corrupted the visibilities. Removing only the worst affected baselines gave acceptable images marred only by weak artifacts concentric with the phase centers of the observations. As before, prior to mosaicking, the prominent unrelated sources in the field were removed. The MEM solution converged with an rms noise estimate of 43 μJy beam^{-1} ($\sim$3 times the theoretical value, limited by dynamic range), producing a Stokes *I* image with a resolution of $3''.8 \times 2''.1$ P.A. $0°.1$. This is shown in Figure 4. Again, the sources subtracted prior to deconvolution have not been added back to the final image, but in this case none fall in the region displayed.

2.2.3. *Mosaicking Stokes Q and U*

Mosaicked images of *Q* and *U* were prepared at 4790 MHz following a procedure similar to that used for the wide-field Stokes *I* mosaic, but using only the data acquired after 1991 August. Since none of the field sources were polarized, it was not necessary to perform the pre-CLEANing stage. The fields were mosaiced using AIPS task UTESS, which—unlike VTESS—does not enforce positively in the solution, which is necessary since *Q* and *U* can be neglective. The final mosaics had resolutions of $10''.8 \times 6''.3$ P.A. $2°.3$, with an rms noise of 65

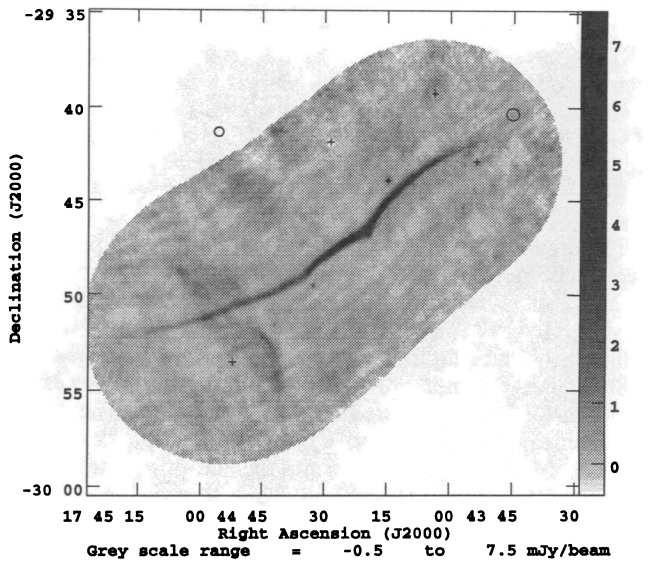

FIG. 3.—The ATCA 4790 MHz mosaic of the Snake. Sixteen observations on four field centers were used to make this image, the resolution of which is $13''.7 \times 7''.2$, P.A. $0°.8$. The cutoff around the edge of this image was set at the point where the primary beam corrected noise exceeded 275 μJy beam^{-1}. Note that unrelated field sources have been subtracted from the ATCA image; the locations of the subtracted point sources are marked with crosses, and the cores of the extended H II regions are marked with circles. These sources are present in the VLA 1446 MHz image of the same region (Fig. 2).

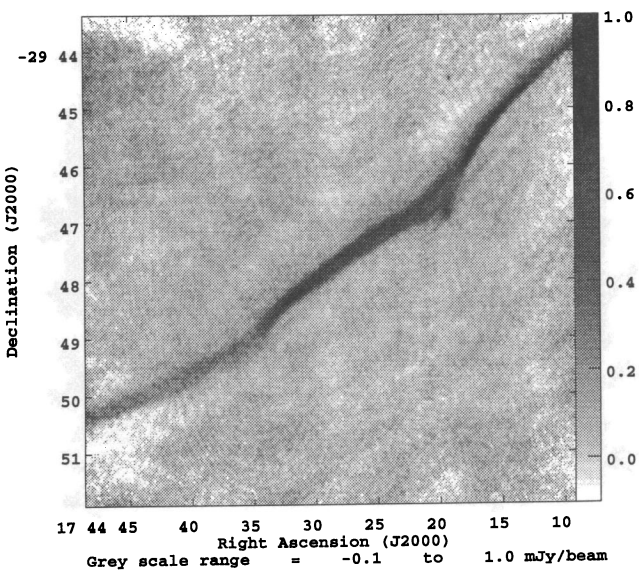

FIG. 4.—The 4790 MHz ATCA high-resolution mosaic of the Snake. This image shows only the central region of the Snake (see Fig. 3) at a resolution of 3.″8 × 2.″1 P.A. 0.°1. As in Fig. 3, unrelated field sources were subtracted prior to making this image (see text for details), but in this case none fall in the region displayed.

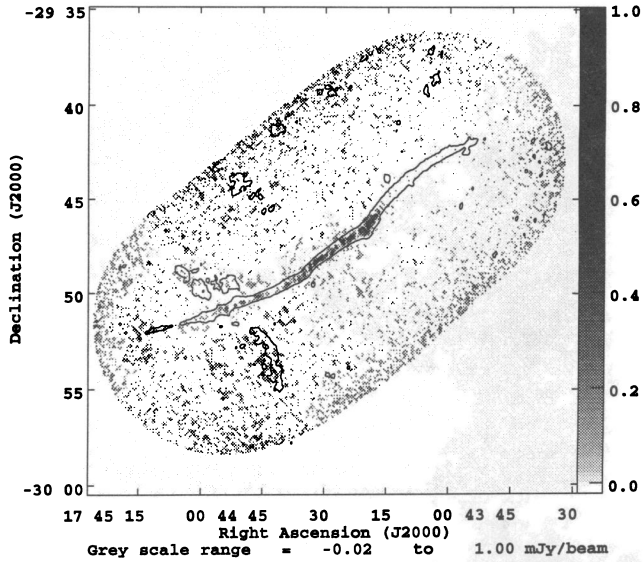

FIG. 5.—The 4790 MHz ATCA mosaic of polarized intensity for the Snake. The contour plotted is the 1 mJy beam^{-1} contour of the total intensity image in Fig. 3, which covers the same region and has nearly identical resolution. This image has been blanked in regions where the polarized intensity falls below 3 times the nominal rms noise. Note the rapid decrease of polarized intensity in the northern part of the Snake.

μJy beam^{-1} per field, or $\sim$2 times the theoretical value. The excess is probably due to low-level sidelobes from polarized sources in the region (such as the SNR G359.1−0.5). Like the Stokes I mosaic, these images were masked where the primary-beam–boosted noise exceeded 5 times the minimum noise of the mosaic, or 260 μJy beam^{-1} in this case. The mosaics were combined to form an image of polarized intensity, $P = (Q^2 + U^2)^{1/2}$ (Fig. 5, blanked where the signal falls below 3 σ to suppress regions of no significant signal), and of the observed polarization angle, $\theta_P = \frac{1}{2}\arctan(U/Q)$ (Fig. 6).

2.2.4. *Spatial and Spectral Variations of Polarization*

Although the data used for the polarimetry were the same as those which produced the acceptable high-resolution Stokes I image, the sampler problem—which manifested itself as a small, spurious, time-variable signal—prohibited the use of any baselines greater than 3.0 km for polarimetry, since I is related to the sum of XX and YY while Q and U are related to the difference (see eqs. [4.45] and [4.46] of Thompson, Moran, & Swenson 1986). Nonetheless, using all baselines shorter than

TABLE 2

SOURCES IN THE VICINITY OF THE SNAKE[a]

Number	Description	References
1.....	Nonthermal filaments of the "Arc"	1, 2, 3
2.....	Thermal "Arches"	2
3.....	Nonthermal "thread" of radio emission	4
4.....	Sgr A complex	5
5.....	Nonthermal filament G359.54+0.18	6, 7
6.....	Sgr C complex (G359.4−0.1)	8
7.....	G359.23−0.82 or "the Mouse"	9
8.....	H II region FIR 27 or G359.28−0.26	10, 11, 12
9.....	H II region G359.186−0.026	13
10.....	SNR G359.1−0.5	12, 14, 15, 16
11.....	"the Snake"	17
12.....	Diffuse object, possibly nonthermal	18
13.....	SNR G359.0−0.9	19
14.....	Sgr E complex	20, 21
15.....	Thermal streamer emanating from Sgr E	22
16.....	VLA calibration source B1741−312	
17.....	Peculiar nonthermal source G357.7−0.1	23, 24, 25
18.....	SNR G357.7+0.3	15

[a] See Fig. 1.

REFERENCES.—(1) Yusef-Zadeh et al. 1984; (2) Yusef-Zadeh 1986; (3) Yusef-Zadeh & Morris 1987a; (4) Morris & Yusef-Zadeh 1985; (5) Ekers et al. 1983; (6) Bally & Yusef-Zadeh 1989; (7) Bally et al. 1989; (8) Liszt 1985; (9) Yusef-Zadeh & Bally 1987, 1989; (10) Odenwald & Fazio 1984; (11) Odenwald 1989; (12) Uchida et al. 1992; (13) Caswell & Haynes 1987; (14) Downes et al. 1978; (15) Reich & Fürst 1984; (16) Uchida et al. 1992; (17) Gray et al. 1991; (18) Anantharamaiah et al. 1991, Fig. 1; (19) Reich et al. 1988, 1990; (20) Liszt 1988, 1992; (21) Gray et al. 1993; (22) Paper I; (23) Helfand & Becker 1985; (24) Shaver et al. 1985a; (25) Caswell et al. 1989.

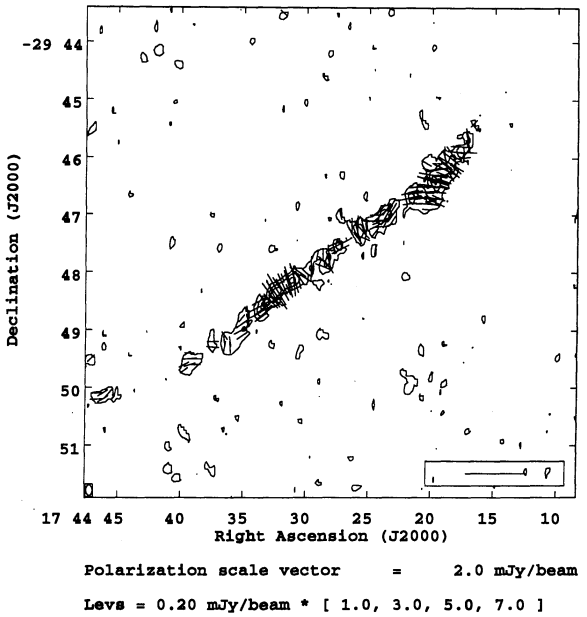

FIG. 6.—Observed polarization angle for the Snake at 4790 MHz. The contours are those of polarized intensity (P), while the line segments are scaled in length to reflect the intensity of the point at the center of the line and are rotated to reflect the polarization angle of the detected electric field ($\theta_P = 0°$ is vertical and increases counterclockwise). Showing the entire length of the Snake with this representation would be too confusing, so the region displayed here corresponds only to the area shown in Fig. 4. This is the region of highest polarization.

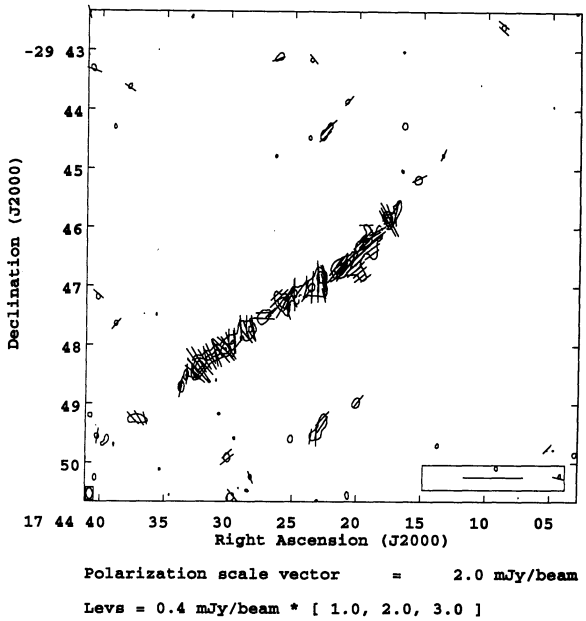

FIG. 7.—Observed polarization angle at 5840 MHz. This representation is the same as that used in Fig. 6, with contours of polarized intensity and line segments representing the angle and amplitude of the polarized electric field incident at the antenna. The polarized intensity was blanked below 2 σ to remove noise before making this plot. The apparent emission to the north and south of the Snake is residual sidelobes and noise boosted by the primary beam correction.

3.0 km (48 kλ) allowed a factor of almost 2 increase in resolution over the Q and U images discussed above. Such images were made with a 100 MHz bandwidth centered at 4790 MHz, and also with 25 MHz subbands centered at 4750 and 4830 MHz (i.e., at either end of the full bandpass) to probe the change of observed polarization with spatial resolution and frequency. For comparison purposes, all three sets of Q and U images were convolved to a common resolution of 8″ × 5″ P.A. 0° before making images of polarized intensity and position angle, to eliminate possible effects arising from slightly differing beam sizes. These images are not presented here since they differ only in details from images already shown.

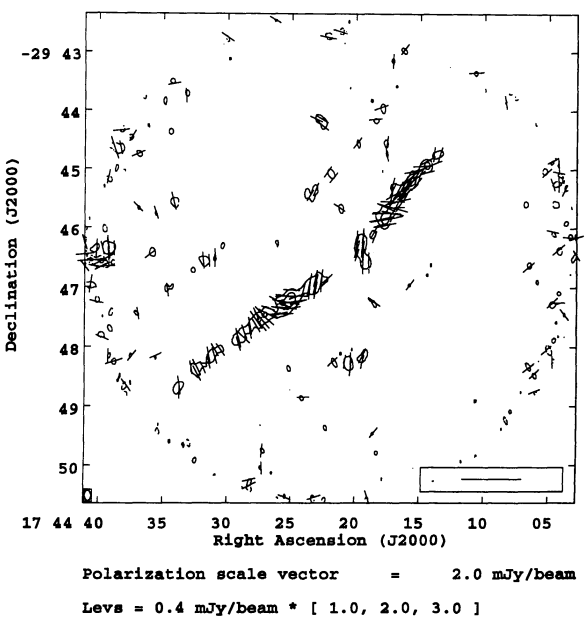

FIG. 8.—Observed polarization angle at 8640 MHz. See the caption to Fig. 7 for comments relating to this representation.

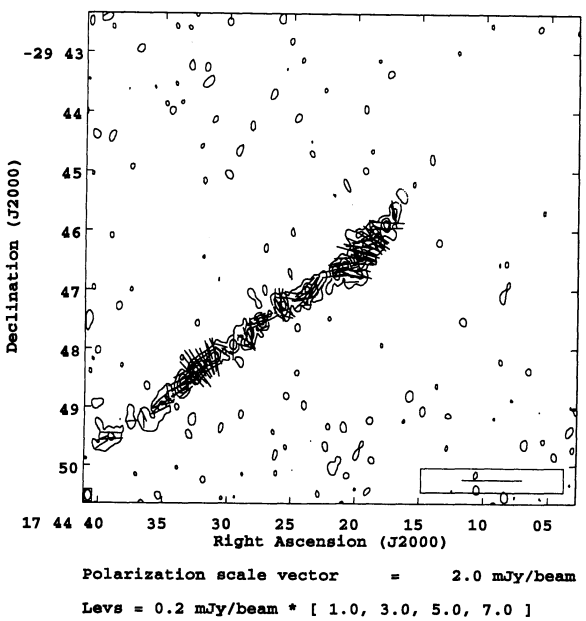

FIG. 9.—Observed polarization angle at 4790 MHz. These are the same data as shown in Fig. 6, spatially rescaled to match the higher frequency data.

2.2.5. *Polarimetry at* 5840 *and* 8640 MHz

Polarimetry was also completed using the 5840 and 8640 MHz data collected in 1993 April. The data were reduced in an analogous way to the 4790 MHz data, and images of Stokes I, Q, and U made. The Q and U images at the two frequencies were convolved to the same resolution as the 4790 MHz polarization mosaic (10.″8 × 6.″3 P.A. 2.°3) and images of P and θ_P prepared. The results are shown in Figures 7 and 8, with the 4790 MHz results to the same spatial scale in Figure 9.

3. DISCUSSION OF STOKES I RESULTS

The Snake lies close to the Galactic plane and less than 1° from the Galactic Center in an area richly populated by unusual objects. A montage of un-CLEANed MOST images of the Snake and the surrounding region is shown in Figure 1. Many of the sources aside from the Snake seen in this image will feature in the discussions which follow.

3.1. *Properties of the Snake*

The Snake is a long, thin (length-to-width ratio ∼150), filamentary object lying almost perpendicular to the Galactic plane at a longitude of $l \simeq 359.°1$. The H I data of Uchida, Morris, & Yusef-Zadeh (1992) indicates that it is probably physically located in the Galactic center, at which distance (8.5 kpc; Kerr & Lynden-Bell 1986) the angular separation from the nucleus corresponds to 130 pc, and its length of 24′ equates to 60 pc. Among similar filamentary features, its length is equaled only by the filaments of the Arc near Sgr A (see, for example, Yusef-Zadeh, Morris, & Chance 1984). Unlike other filaments in the region, however, the Snake lies at southern Galactic latitudes—terminating ∼3′ below the plane—and does not curve smoothly and monotonically, instead displaying abrupt changes of curvature or kinks. These are located at G359.13−00.19 [$17^h44^m19^s.54$, −29°46′47.″0 (J2000.0); hereafter referred to as "the major kink"] and at G359.12−00.26 [$17^h44^m34^s.68$, −29°49′05.″0 (J2000.0); "the minor kink"]. At the cusp of the major kink there is an enhancement in emission, which is not seen in the minor kink, although an unresolved source does lie nearby. It is not clear if this latter source is related to the Snake. Aside from a possible weak interaction with SNR G359.1−0.5 (discussed further in § 3.3.2) the Snake seems to be an isolated feature with no obvious external powering source.

The higher resolution data (Fig. 4) show that the enhancement at the cusp of the major kink consists of a weak (∼0.1 mJy) unresolved component surrounded by a diffuse halo-like structure. These data also reveal that the "body" of the Snake is composed of three or more subfilaments (see Fig. 10). The subfilaments diverge slightly as they are traced northward from the minor kink, reaching a total width of 20″. Some complex structure is evident near the cusp of the major kink, beyond which the subfilaments merge to form the northern arc. That arc is well resolved with an intrinsic width of 7″ and shows some evidence of double structure. Similar multiple structure is also seen (although less clearly) south of the minor kink in the superresolved VLA image (Fig. 11). Such multiple structure is not unique, and is seen in the filaments of the Sgr A Arc (see, for example, Yusef-Zadeh et al. 1984; Yusef-Zadeh 1986; Yusef-Zadeh & Morris 1987a) and the isolated double filament G359.54+0.18 (Bally & Yusef-Zadeh 1989; Bally et al. 1989).

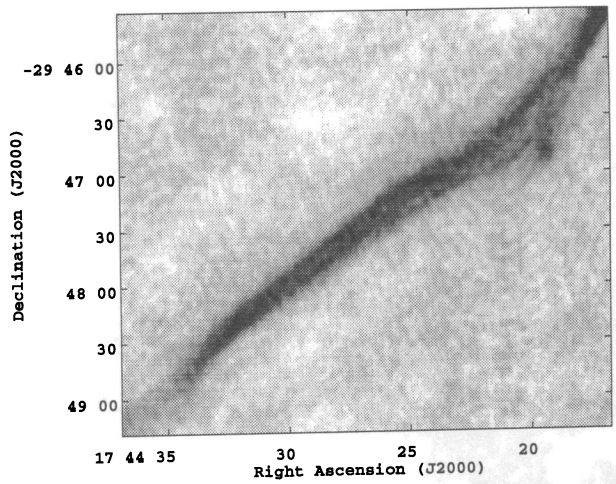

FIG. 10.—Substructure in the Snake at 4790 MHz. This is a contrast-enhanced ATCA image prepared from the same data shown in Fig. 4. It shows a close-up of the region between the two kinks at a resolution of ∼4″ × 2″. Note the presence of several straight and curved filaments within the Snake itself. The "speckled" appearance is not believed to be a property of the source, but arises from residual artifacts described in the text (§ 2.2.2).

3.1.1. *Intensity and Spectral Index Distributions*

The distributions of intensity and spectral index were determined from cross-cuts at 1′ intervals along the length of the Snake made from both the 1446 and 4790 MHz images convolved to a common resolution of 20″ × 20″. A linear base level was removed from each cross-cut before using the peak intensity to generate plots of the latitude distribution of flux density and spectral index (Fig. 12; note that the sign convention for spectral index α is in the sense that $S_\nu \propto \nu^\alpha$). From this plot it appears that the Snake has a negative spectral index within the rim of G359.1−0.5 (latitude $< -22'$) and a flat spectrum up to the minor kink ($-16'$). The intensity then rapidly increases and the spectrum steepens toward the major kink ($-12'$) before flattening or inverting at the northern end. It should be noted that the end-most points are possibly still affected by confusion and dynamic range effects due to the nearby extended sources and may not accurately reflect the true spectral distribution.

Reich & Schlickeiser (1992) have measured the spectral index of the Snake between 10.55 and 32 GHz, finding

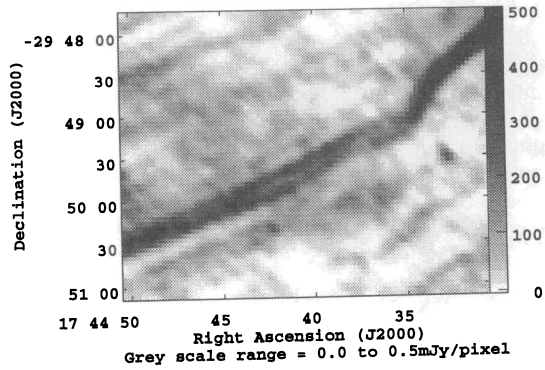

FIG. 11.—Substructure in the Snake at 1446 MHz. This is a superresolved VLA image prepared from the same data shown in Fig. 2. It shows a close-up of the region south of the minor kink. Note the presence of several straight and curved filaments within the Snake itself.

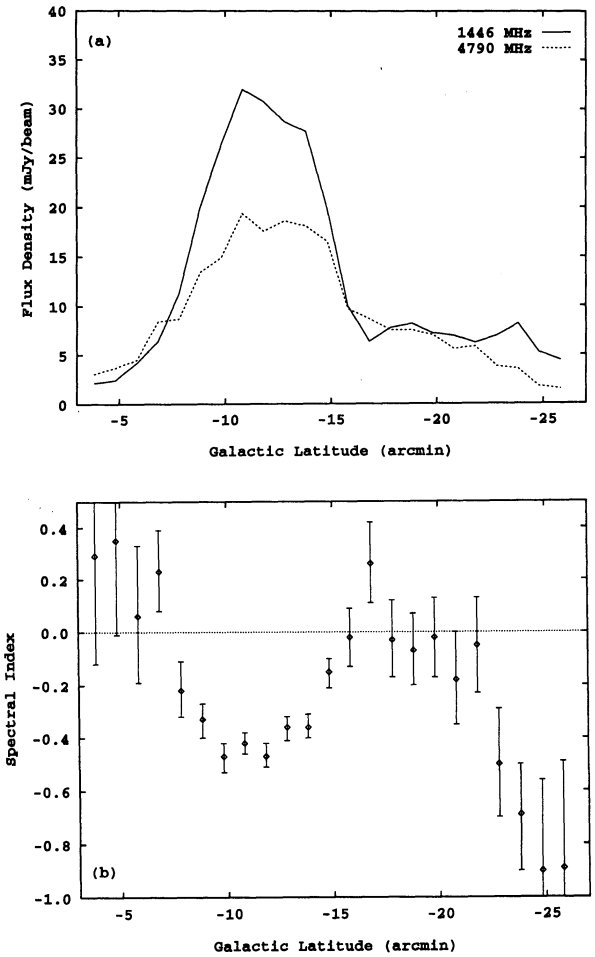

FIG. 12.—Latitude variation of (*a*) the flux density at 1446 and 4790 MHz and (*b*) the implied spectral index of the Snake.

$\alpha = -0.2 \pm 0.2$. The Snake is also present in the 330 MHz VLA data of Pedlar et al. (1989) and Anantharamaiah et al. (1991), but in those data—as with the MOST data—the resolution is an order of magnitude lower ($\sim 1'$), and so direct comparison with the higher frequency data is difficult. Furthermore, at 330 MHz there are considerable dynamic range problems due to the many nonthermal sources in the region. Nonetheless, the indication from this and the MOST data is that at frequencies below ~ 1 GHz the spectral index becomes very negative ($\alpha < -1$). This has been modeled in terms of a two-component system; a halo whose electrons have a normal power-law energy distribution, giving rise to a steep low-frequency spectrum, plus a core component whose electrons have a power-law energy distribution with a low-energy cutoff, producing a turnover at higher frequencies. The combination of these components yields the observed spectrum (Nicholls & Gray 1993).

3.1.2. *Minimum Energy and Magnetic Field*

A modified form of the model proposed by Killeen, Bicknell, & Ekers (1986) for jets of Gaussian profile in radio galaxies was used to determine minimum energy and magnetic field estimates for the Snake, modeled as a cylinder having Gaussian density profiles in both latitudinal and longitudinal directions. The following parameters were assumed:

latitudinal FWHM:	σ_x	$= 9''.4$,
longitudinal FWHM:	σ_y	$= 300''$,
peak surface brightness:	I_ν^0	$= 0.1175$ mJy arcsec^{-2},
observing frequency:	ν	$= 4790$ MHz,
lower spectrum cutoff:	ν_l	$= 10$ MHz,
upper spectrum cutoff:	ν_u	$= 100$ GHz,
spectral index:	α	$= -0.4$,
geocentric distance:	R_0	$= 8.5$ kpc,
energy ratio:	k	$= 1$,

where the energy ratio k is the ratio of the energy in relativistic protons and thermal particles to that in relativistic electrons. The corresponding parameters for the Snake were found to be

minimum energy:	$E_{\rm min}$	$= 4.7 \times 10^{46}$ ergs,
minimum magnetic field:	$B_{\rm min}$	$= 8.8 \times 10^{-5}$ G,
minimum pressure:	$P_{\rm min}$	$= 3.8 \times 10^{-11}$ dynes cm^{-2},
synchrotron luminosity:	$\dot{E}$	$= 1.8 \times 10^{33}$ ergs^{-1},
synchrotron lifetime:	τ_s	$= 7.9 \times 10^5$ yr.

The speed at which the electrons diffuse along the magnetic field lines is limited by the Alfvén speed (Alfvén 1942), which for the equipartition magnetic field strength above and a thermal electron density of 10 cm^{-3} (which will be derived below in § 4.2.1) is $v_A = 0.6 \times 10^2$ km s^{-1}. The time for electrons to diffuse the entire length of the Snake, or 60 pc, is then ~ 1 Myr, or comparable to the synchrotron lifetime. Thus the source of relativistic electrons cannot be localized by this means.

3.1.3. *Dynamical Timescales*

The timescale on which the Snake will remain relatively undisturbed is limited by differential rotation and the bulk motions of molecular clouds in the region. Using the Galactic rotation law derived by Sanders (1989), at a galactocentric radius of 130 pc—the Snake's mean projected separation from the nucleus—the period of one revolution around the nucleus is 3.65 Myr. This varies by ± 0.05 Myr at the inner- and outermost parts of the Snake's slightly kinked structure. The variation in period is thus less than 2% across the radial extent of the Snake, so—assuming that over the length of the Snake there is negligible variation of rotation rate with distance from the Galactic plane—the feature will be stable to differential rotation over several times the 0.8 Myr synchrotron lifetime. A similar argument perhaps explains why it is that filamentary features are only seen perpendicular (or nearly so) to the Galactic plane; a filament of the same length as the Snake and centered at the same longitude but oriented radially suffers differential rotation with the periods of the two ends differing by ~ 1.5 Myr. Such a feature would be destroyed rapidly.

It has been argued (Yusef-Zadeh & Morris 1987b, c; Morris 1990) that the magnetic field in Arc filaments must be of milliGauss strength or greater in order for their rigidity to withstand the ram pressure of the clouds and retain their coherence despite spanning scales much larger than the expected turbulence in the interstellar medium. The magnetic field in the Snake is possibly weaker by up to an order to magnitude, so the motions of molecular clouds might produce some distortion. These motions are $\lesssim 10^2$ km s^{-1} (Blitz et al. 1993), so if the Snake were initially a perfectly linear structure it would take a cloud moving at this velocity $\gtrsim 10^4$ yr to produce the

current distortion. This is much shorter than the timescale for disruption by differential rotation, and could limit the age of the Snake to be considerably less than the upper limit on the Alfvén diffusion time (~1 Myr) unless it is far more distorted than it appears in projection, which seems unlikely. Since these values are only limits, however, it is not possible to place tight constraints on the positions of possible localized illuminating source(s) based on diffusion time arguments.

3.2. *Comparison with Similar Objects*

Filamentary objects have been known in the Galactic center for some time (see, for example, Yusef-Zadeh et al. 1984; Morris & Yusef-Zadeh 1985; Bally & Yusef-Zadeh 1989), and appear to be unique to this environment: only half a dozen examples are known, with none lying further than ~1° from the nucleus. The extensive MOST Galactic Plane Survey (Whiteoak et al. 1989) has revealed only one object near the Galactic plane but outside the Galactic center with any morphological similarities (G286.5−01.2; see Whiteoak & Green 1993b). This feature appears to be merely the brightest portion of a much larger nonthermal structure, however, and is probably part of a supernova remnant, while the Snake and other Galactic center filaments are isolated features.

It appears that something unique to the Galactic center must provide the necessary conditions for formation and/or illumination of these objects. Even in this environment, however, the Snake is set apart from other filaments by several properties: (1) it is the longest isolated quasi-linear feature, equaled in length only by the filaments of the Arc near Sgr A; (2) unlike the other filaments, it is not monotonically curved and shows prominent kinks; (3) the intensity distribution does not fade monotonically toward its end as do those of other filaments; (4) it is further from Sgr A, the presumed center of activity in the Galactic center, that any other known filamentary structures; (5) it lies outside the so-called Galactic center Lobe (Sofue & Handa 1984), in the interior of which all other known threads or filaments exist (Anantharamaiah et al. 1991); (6) aside from some weak filaments associated with the Arc (Yusef-Zadeh et al. 1990), the Snake is the only known thread or filament which exists entirely at southern Galactic latitudes.

Despite these differences, there are also similarities when the Snake is compared with other filaments in the region. The spectral index found for the Snake between 1446 and 4790 MHz is consistent with the other filaments, for which the 330/1400 MHz spectral indices are in the range $-0.8 < \alpha < -0.04$ (Anantharamaiah et al. 1991). The minimum magnetic field determined for the Snake (§ 3.1.2) is also similar to the several tens of micro-Gauss found for the other filaments and threads (see Anantharamaiah et al. 1991), in each case an order of magnitude greater than the expected field in the Galactic disk (see, for example, Blitz et al. 1993). These similarities and its proximity to the other filaments and their uniqueness to the Galactic center means that it is highly probable that the Snake arises from similar physical processes. The unusual morphology that we see may result from intrinsic differences in the Snake's formation, or it may be a result of interactions with nearby objects. We now address the question of the origin of the Snake.

3.3. *Origin of the Snake*

There has been considerable debate on the origin and powering of Galactic center filaments. Those found near Sgr A (the threads and the Arc) are conjectured to be powered by Sgr A, which dominates the energetics of the region, although they are not obviously connected to it. Some possible origins of filamentary structures are discussed by Morris & Yusuf-Zadeh (1985). These and other means of producing long narrow filamentary objects are now briefly discussed in the context of the Snake.

3.3.1. *Jets or Ejecta from SNRs*

At its southern end the Snake crosses the shell of SNR G359.1−0.5 and is oriented nearly radially outward from the shell's center, suggesting that it may be the result of some phenomenon related to the supernova event. Radial protrusions from SNRs are not unprecedented (Kesteven et al. 1987; Caswell et al. 1987; Yusef-Zadeh & Bally 1987, 1989), but no known examples resemble the Snake in terms of morphology or brightness distribution. Furthermore, the Snake penetrates some 5′ into the shell interior rather than terminating at or merging with the shell. Other filaments in the Galactic center region, with which the Snake otherwise has much in common, do not have obvious links to SNRs at all, so an SNR-based explanation cannot have general applicability.

3.3.2. *G359.1−0.5 and the Snake*

Although the Snake is unlikely to be a jet or ejecta phenomenon, it may be undergoing some form of interaction with G359.1−0.5. H I absorption measurements show that both lie at a similar distance (Uchida, Morris, & Yusef-Zadeh 1992), and at frequencies above 1.4 GHz the rim of G359.1−0.5 is brighter near its intersection with the Snake, which has been taken as evidence of an exchange of energy between the two (Uchida, Morris, & Yusef-Zadeh 1992). This hypothesis is supported by the MOST image of G359.1−0.5 (Fig. 1 and Paper II), which shows no brightening of the shell near the Snake, implying a flatter spectrum there. The spectral index of the Snake also appears to be close to zero in that region (Fig. 12). Furthermore, where the Snake crosses G359.1−0.5 it suffers a slight but abrupt change of direction by roughly −9° in position angle, although the Snake also displays abrupt changes of direction elsewhere, notably at the kinks.

3.3.3. *Star Wakes or Trails*

Energy deposited in the interstellar medium by a massive, relativistically moving object could cause the prompt formation of a wake (see Yusef-Zadeh & Bally 1987). For the Snake there is no evidence of the head-tail appearance expected of such a system. An alternate model involves the supersonic passage through the interstellar medium of a star with a massive stellar wind. An injection of energetic particles by, for example, a subsequent supernova explosion which intersects the trail might than cause its illumination. Such a model has been explored for the "chimney" in the Crab nebula (Blandford et al. 1983; Cox, Gull, & Green 1991), and has also been proposed for the Snake (Nicholls & Le Strange 1995). While it readily explains the long, thin structure of the Snake—and perhaps also explains the kinks as evidence of close encounters of the star with massive objects—there are some known properties of the Snake which cannot yet be understood in the current model.

One argument against a star trail model is that, since the Snake is so similar to other filaments in the region, one might expect it to have a similar genesis. An SNR-illuminated star trail explanation for all of the filaments is, however, difficult to conceive, since no others have nearby SNRs. It cannot be ruled out, however, that some other mechanism could be providing

the energetic particles to illuminate the trails. More difficult to overcome is that fact that some filaments exhibit curvatures which are not consistent with the expected trajectories of stars on radial orbits, for example being convex toward the nucleus rather than away from it. If the Snake is a star trail and these other filaments are of a different origin then one must explain how the two types of objects end up with such similar gross properties.

3.3.4. *Shock Fronts*

Shock fronts were considered and dismissed by Morris & Yusef-Zadeh (1985) since the coherence of structure over a distance of ~ 30 pc is inconsistent with the inhomogeneous interstellar medium in the Galactic center. The shock front model also requires that the shock surface must be seen edge-on in order to give a linear appearance. The number of linear objects known implies that there must be many more unseen shocks which are not edge-on. All the known filaments are, however, more consistent with tube- or threadlike structures than edge-on sheets, although a shock model of the Arc has nonetheless been formulated (Bally et al. 1988), in which a molecular cloud on an inclined, elliptical orbit is colliding with a cloud in the plane. Clouds consistent with this are known to exist in the Arc region, but in the case of the Snake the clouds traced by ^{12}CO (Uchida et al. 1992) show a void in the vicinity of the Snake.

3.3.5. *Cosmic Strings*

Cosmic strings are believed to behave as super-conductors and should therefore have strong electromagnetic interactions with plasmas, developing large currents. It has been suggested that they would be visible as synchrotron sources (see Chudnovsky et al. 1986 and references therein). Models of particular astronomical objects as string-related phenomena have been made (Vilenkin & Field 1987; Vilenkin 1988), and Chudnovsky et al. (1986) and Manka & Bednárek (1991) have discussed Galactic phenomena in this context, including the Galactic center threads (Morris & Yusef-Zadeh 1985). The latter is of particular relevance here since the Snake has much in common with the threads.

Chudnovsky et al. (1986) model the observed radio emission from the threads as being from a cosmic string with magnetic field strength ~ 3 μG and a length of $\sim 3 \times 10^{20}$ cm. The derived minimum magnetic fields in the threads are all 50–100 μG (see Anantharamaiah et al. 1991) and the greatest length is that of the Snake, at $\sim 2 \times 10^{20}$ cm. For a magnetic field of ~ 90 μG and an electron density of ~ 10 cm^{-3}, the expected luminosity for the Snake modeled as a cosmic string exceeds the observed luminosity by more than 6 orders of magnitude. Furthermore, cosmic strings should move relativistically at a speed $v = c/2^{1/2}$ (see, for example, Chudnovsky et al. 1986). At a distance of 8.5 kpc a proper motion of up to $\sim 5''$ yr^{-1} would therefore be expected. MOST data on the Snake date back to 1983 and higher resolution VLA/ATCA data are available from 1990. None of these data show the expected motion of up to 50″ to the present day, with a limit of $\lesssim 0\farcs5$ yr^{-1} ($v \lesssim 0.1c$). This rules out a cosmic string explanation for this object unless the majority of the motion is in a place close to the line of sight along the entire length of the Snake.

3.3.6. *The Great Annihilator* (1E1740.7−2942)

Reich & Schlickeiser (1992) have speculated that the Galactic center positron annihilation source "the Great Annihilator" (1E1740.7−2942; see Mirabel et al. 1992) and the Snake have a common origin, with the Snake representing past activity and 1E1740.7−2942 being the present location of the energizing source. However, 1E1740.7−2942 is displaced some 2′ (~ 5 pc) perpendicularly from the long axis of the Snake with no visible evidence of a connecting path. Furthermore, no γ-ray sources are located close to the other threads and filaments, to which the Snake is closely similar in all other properties. In the absence of compelling evidence to link 1E1740.7−2942 to the Snake, the suggested association is rejected.

3.3.7. *Morphologically Unusual SNRs*

A model of the evolution of an SNR in a highly magnetized medium has been developed by Insertis & Rees (1991), in which expansion is constrained by the magnetic field, producing a long, thin structure. The authors speculated that the threads discovered by Morris & Yusef-Zadeh (1985) might be manifestations of such SNRs. The Snake might then also be a candidate, except that the SNR G359.1−0.5 is believed to lie at a similar distance (Uchida, Morris, & Yusef-Zadeh 1992) yet is almost perfectly circular. It is difficult to conceive of a situation where two adjacent SNRs would have such different morphologies, so such an explanation is unlikely.

3.3.8. *Electrodynamic Activity*

Several models of electrodynamic phenomena at the Galactic center have been developed. One argument put forward by Heyvaerts, Norman, & Pudritz (1988) is that electrodynamic activity in the Galactic center occurs within and on the surface of the Galactic center lobe (GCL; Sofue & Handa 1984). Since the Snake lies well outside the GCL, however, this model—as it stands—cannot explain its presence. Whether this is fatal to the entire theory is not clear. A second argument (Benford 1988) relies on currents generated along ~ 100 pc paths in a highly ordered milli-Gauss magnetic field. The filaments delineate current paths that have been pulled away from the more active regions by magnetic tension. It is not clear from where the Snake might have been "pulled," since Sgr A is ~ 130 pc away with no obvious return current path, but if Sgr A is the source and the Snake is no older than a few times 10^4 years—as suggested by dynamical arguments above and consistent with the ohmic time scale of the generator (Benford 1988)—then its transverse proper motion could be as large as a few times $0\farcs1$ yr^{-1}. Such motion is below current detection limits, but an observable limit will be available within a reasonable time. Benford's model also raises the possibility of rapid (~ 2 yr) flares and suggests that there may be many more, much fainter filaments. There is as yet no evidence for substantial variability in data collected to date, but the possible existence of proper motion and flares makes monitoring these objects a potentially profitable enterprise.

3.4. *Summary*

Whatever the powering source, it is most likely that the long, thin morphology of the filaments and threads is dominated by the local magnetic field—the previously known filaments roughly delineate a poloidal field (Yusef-Zadeh & Morris 1987a; Anantharamaiah & Pedlar 1990), which presumably permeates the entire region, so the similarity of the Snake's physical properties to these objects suggest that it too is magnetically dominated. The reason for the illumination of selected field lines is attributed to localized energy release by Morris & Yusef-Zadeh (1985), although what phenomenon is releasing that energy is unclear.

The key to understanding the Snake in particular would seem to rest with the kinks—no other similar objects have them, and none resemble the Snake in a detailed comparison. Many of the differences seem to center around the kinks: as well as the abrupt change of direction three is also a change in the filamentary substructure at both kinks and a substantial change in brightness at the minor kink and a smaller one at the major kink. Few of the models discussed above provide a ready means of explaining this kinking in the context of the known properties of the Snake—jets and ejecta from SNRs should presumably travel in straight lines, as should stars leaving trails or wakes, although one might argue that passage close by a massive object might cause a perturbation of the path which, when viewed from some angle, might resemble the observed kinking. Shock fronts could conceivably display such kinks, but other considerations would seem to rule out this and the above-mentioned models (see above). Similarly, the cosmic string, Great Annihilator, and unusual SNR models also do not readily explain the kinking and also suffer from other flaws which are probably fatal in any case. The remaining model discussed here, electrodynamic activity, does not rule out nonlinear morphologies (see, for example, Benford 1988), however, and also is consistent with other properties of the filaments. It is thus the favored explanation at present.

More detailed studies of this the Snake are planned, including observations of the interactions taking place near and at the kinks using higher sensitivity and resolution than so far achieved.

4. DISCUSSION OF POLARIMETRY RESULTS

Contrary to indications at 1446 MHz, the Snake shows fractional polarization up to 24% at 4790 MHz, thus confirming that its emission is nonthermal. However, the detected polarisation suddenly faces ~1′.5 north of the major kink (see Figs. 5 and 13), with any polarization in the "missing" northern portion lying below the instrumental sensitivity. Aside from the northern arc, the detected polarization traces the total intensity emission well, but is clumpy, with the polarization vectors showing large changes of angle between clumps (see Fig. 6).

Although the sharp change in polarization might indicate a change in the emission properties, the overall similarity in total intensity between the southern and northern portions of the Snake and their continuity of structure makes it unlikely that they could be dominated by different emission mechanisms. Moreover, the 330 MHz data of Anantharamaiah et al. (1991) show the northern section strongly in emission, implying a nonthermal nature despite it apparent lack of polarization. The small-scale variations in polarized intensity also do not reflect variations in total intensity. We thus hypothesise that the large- and small-scale variations are both due to depolarization; rotation measures of several thousand radians per square meter are known in nearby regions (Tsuboi et al. 1986; Yusef-Zadeh & Morris 1987b). The higher frequency ATCA data support this hypothesis: at 8640 MHz (Fig. 8) the emission is less clumpy and ~50% polarized, with an northward extent greater than either 4790 MHz (Fig. 9; 24% polarized) or 5840 MHz (Fig. 7; fractional polarization similar to 4790 MHz). This is also consistent with the 10.55 GHz data of Reich & Schlickeiser (1992), where a polarized fraction of 60% was reported, with a northward extent comparable to the 8640 MHz result reported here (precise details are unclear since the resolution of the 10.55 GHz data is only 1′.2).

The increase in spatial extent and polarized fraction with increasing frequency is expected if strong Faraday rotation effects are at play, since these effects vary with the square of the wavelength (see, for example, Burn 1966). An alternative explanation by Reich & Schlickeiser (1992) suggests that the fall-off of polarization arises from a sudden change in the geometry of the magnetic field to produce a very small-line-of-sight component, but we see no evidence which favors this explanation over the Faraday effect. A more detailed discussion of the Faraday rotation model is now presented.

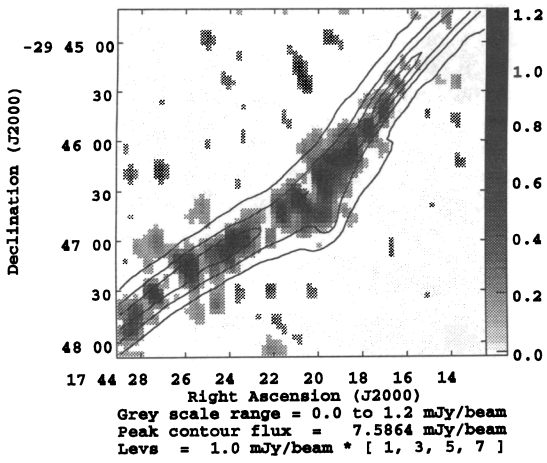

FIG. 13.—Detailed view of the disappearance of polarization north of the major kink. The kink is near the center of the image. The gray scale is of polarized intensity, with superimposed contours of total intensity. Note that the polarized intensity fades and vanishes near the point where the total intensity is maximum.

4.1. *Depolarization Effects*

Three main effects cause depolarization (see, for example, Burn 1966): (1) in the presence of spatially varying polarization angles—either intrinsic or due to spatial variations in rotation measure—a spatial convolution with a nonzero beam width can result in a decrease in the intensity of the detected polarized signal due to the inherent vector-averaging; (2) in the presence of large rotation measures, the variation of the frequency-dependent observed polarization angle across a nonzero bandwidth again results in vector-averaging and a consequent decrease in detected polarization; and (3) internal depolarization may occur if the synchrotron and thermal plasmas are spatially coincident, in which case vector-averaging occurs when radiation from different parts of the source on the same line of sight, which will be affected by different rotation measures, combine. The first two effects are, essentially, instrumental and may be combatted at a given frequency by using smaller beams and/or narrower bandwidths, but in the latter case the radiation is depolarized at the source and polarization can only be recovered by using a higher frequency, which reduces the Faraday rotation. Each of these effects is now dicussed in the context of the polarization results on the Snake.

4.1.1. *Beam Depolarization*

The higher resolution 4790 MHz polarimetry (§ 2.2.4) was compared with the initial lower resolution work (Figs. 5 and 6). No significant changes in polarization were observed other than the simple increase in spatial resolution, ruling out beam depolarization as a significant factor in defining the structure

and extent of polarized emission. The clumpiness of the polarized emission cannot be intrinsic to the source, however, since the total intensity is so smooth, and the fact that there are large changes in polarization angle between clumps suggests that they are the result of beam depolarization at boundaries of discrete cells. These cells must be due to structure in an intervening medium which is causing Faraday rotation, and have a scale size of 5″–10″, corresponding to a physical size of 0.02–0.05R, where R is the barycentric distance in kiloparsecs. At the distance of the Galactic center (8.5 kpc) this scale size is 0.2–0.4 pc. Angle shifts of at least 90° are occurring between clumps, which requires rotation measure fluctuations of at least 400 rad m^{-2} between cells.

4.1.2. *Bandwidth Depolarization and Rotation Measure*

A rotation measure of 400 rad m^{-2} produces a differential rotation angle of 3° across a 100 MHz bandwidth at 4790 MHz, corresponding to a depolarization of only 0.05% (see Gardner & Whiteoak 1966). This is a lower limit, however, and a rotation measure of $\sim 10^4$ rad m^{-2} would totally depolarize the radiation. To determine the rotation measure, the polarization images made from narrow subbands centered at 4750 and 4830 MHz (§ 2.2.4) were compared to each other and the 4790 MHz full bandwidth images. Unexpectedly large differential angles were found—up to ~40° near the northern end of the detected polarization (Fig. 14)—implying rotation measures in the range ~2–5.5 × 10^3 rad m^{-2}, increasing toward the Galactic plane. This easily accounts for the absence of detectable polarization in the 1446 MHz data, but is not sufficient to cause more than ~10% depolarization over the 100 MHz bandwidth at 4790 MHz. Unless the rotation measure rapidly doubles north of the major kink, we find that bandwidth depolarization cannot play a major role in defining the structure and extent of the polarized emission from the Snake.

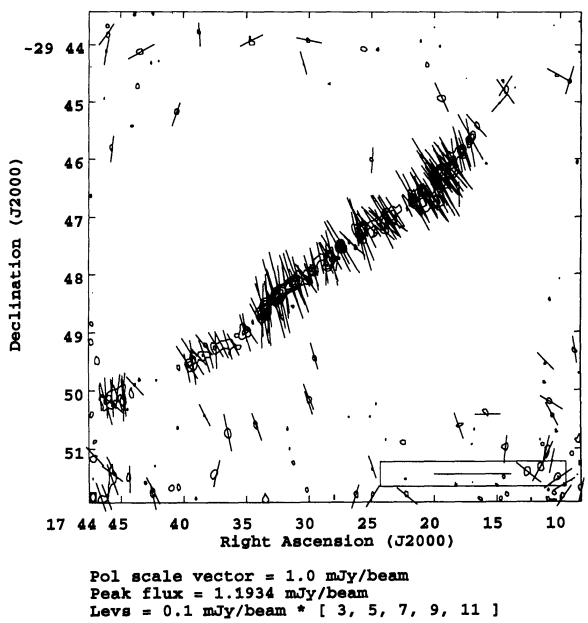

FIG. 14.—Rotation angle between 4750 and 4830 MHz. This plot was produced by differencing the polarization angle at these two frequencies ($\psi_{4750} - \psi_{4830}$). A rotation of zero is represented by a vertical line; positive rotations are anticlockwise in this representation. The contours are of the 4790 MHz (100 MHz bandwidth) bandwidth polarized intensity, which was also used to scale the vector length. The significance of this plot is discussed in the text.

The results found here are consistent with the distribution of polarization angles found at 10.55 GHz by Reich & Schlickeiser (1992), although those authors argued for an upper limit of ~2000 rad m^{-2} toward the Snake on the basis of the high fractional polarization (60%) observed at 10.55 GHz. However, 5.5 × 10^3 rad m^{-2} would only produce a few percent depolarization across their 300 MHz bandpass, and the angle shift induced by the derived rotation measure fluctuations of 400 rad m^{-2} is only 18° at 10.55 GHz, so the expected depolarization in their 1.2 beam due to fluctuations of this magnitude on the scale of ~10″ is only 5% or so. Their limit is thus too conservative.

Very large rotation measures of the magnitude found here are not unprecedented. Extragalactic sources such as Cygnus A show rotation measures of up to 4000 rad m^{-2}, although there the responsible magneto-ionic medium is not believed to lie within our Galaxy (Dreher, Carilli, & Perley 1987). For Galactic sources such as the Snake, however, that medium *must* lie in the Galaxy. Aside from the Snake, to date such high Galactic rotation measures have only been reported for the filaments of the nonthermal Arc feature very close to Sgr A, specifically the feature known G0.16−0.14, for which rotation measures in the range −2000 to −5500 rad m^{-2} were found (Yusef-Zadeh & Morris 1987b). Aside from a change of sign, which merely reflects a reversal of the line-of-sight magnetic field, this range of rotation measures is identical to that found for the Snake. There are other similarities too: both objects show clumpy polarized structure which does not fully trace the extent of the total intensity, and in both the smoothness and extent of the detected polarization increases with frequency (see Yusef-Zadeh 1986; Inoue et al. 1989; Reich 1989). In the case of the Arc it was suggested that the thermal helical filaments reported by Yusef-Zadeh et al. (1984) are likely candidates for the Faraday rotating medium (Yusef-Zadeh & Morris 1987b). No such features are seen near the Snake, suggesting that the region of high Faraday rotation extends over a larger region of the Galactic center. This topic is explored further in § 4.2.1.

4.1.3. *Intrinsic Magnetic Field Orientation*

While knowledge of the rotation measure in principle allows the determination of the intrinsic direction of the magnetic field, in our data the frequency range over which the rotation measure has been estimated is very small ($\Delta\nu/\nu_{\rm avg} < 2\%$). Extrapolation of these results to infinite frequency (zero wavelength) to derive the intrinsic polarization angle—and thence the magnetic field orientation—is difficult, because small uncertainties in the angles at each frequency propagate to a large uncertainty in the extrapolated angle (~1 radian here). The higher frequency ATCA data have provided little extra constraint, since they are of lower quality due to sparse u-v coverage. All that can be said at this stage is that the data are consistent with a magnetic field oriented parallel to the long axis of the Snake.

4.1.4. *Internal Depolarization*

Since neither beam nor bandwidth depolarization effects alone appear to account for the absence of polarization north of the major kink, the remaining possibility is internal depolarization. This effect can be considered in terms of a simple model in which the physical depth of the Snake is modeled as a uniform slab of co-existing nonthermal, synchrotron-emitting and thermal, Faraday-rotating plasmas. It is trivial to show that such a model does not affect the observed polarization angle, but that the intensity of polarized emission leaving the

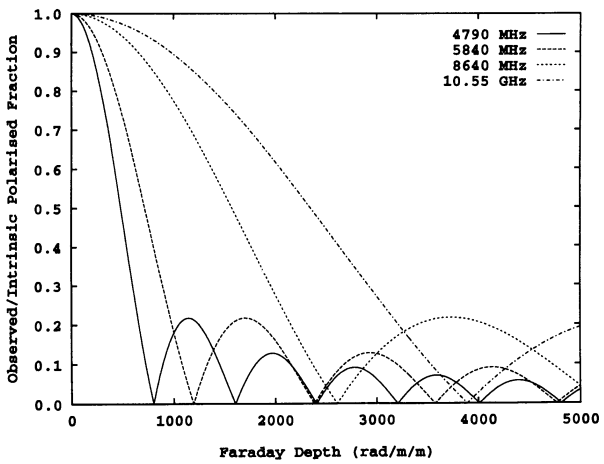

FIG. 15.—Internal depolarization for a uniform slab model, plotted against total Faraday depth for the three frequencies used in this study. Of particular importance is the region below 2000 rad m^{-2} where the 4790 and 5840 MHz curves are comparable but much smaller than the 8640 MHz curve.

source varies with frequency (see Burn 1966). Figure 15 shows the depolarization predicted by this model for the frequencies under study here, plotted against the total Faraday depth through the source (which is *not* the observed rotation measure).

A Faraday depth of $\sim$1400 rad m^{-2} puts both 4790 and 5840 MHz at comparable low amplitudes, while the 8640 MHz and 10.55 GHz curves are considerably higher, the behavior observed in the region immediately north of the major kink (see Figs. 7–9). In numerical terms, assuming an intrinsic fractional polarization of 70%, the model predicts that both 4790 and 5840 MHz would have fractional polarizations of 11%, with 42% at 8640 MHz, and 56% at 10.55 GHz. The latter two values agree with observation, but 11% at 4790 MHz is somewhat higher than the observed polarized fraction in this area. As pointed out by Burn (1966), however, depolarization due to a random or turbulent component of the magnetic field is most important when the steady component of the magnetic field is nearly perpendicular to the line of sight, a field configuration that may well exist in the Snake. A more realistic model incorporating turbulence in the magnetic field will produce depolarization curves that are similar to the nonturbulent case down to $\sim$50%, but then fall off more rapidly and smoothly (see Burn's Fig. 2).

To generate an internal Faraday depth of the magnitude suggested here requires a thermal electron density of $\sim$10 cm^{-3} pc over a path of length $\sim$1 pc, or the approximate width of the Snake, with the assumption that the line-of-sight magnetic field strength is $\sim$90 μG (the minimum magnetic field strength derived above). This thermal electron density is plausible, and is 6 orders of magnitude below the thermal electron density required to render the source optically thick at 330 MHz, at which frequency it is known not to be in absorption (see Anantharamaiah et al. 1991). This high internal Faraday depth only applies north of the major kink, however, and must fall quickly to $\sim$500 rad m^{-2} south of the major kink in order to explain the properties of the polarization detected there. This variation of Faraday depth by a factor of almost 3 over such a short distance could be due to sudden variations in thermal electron density and/of line of sight magnetic field strength—and there are no currently known indicators to refute this explanation—but this variation can be readily explained if we consider the Snake as a ribbon rather than a threadlike feature. It is possible to picture the major kink as a twisting of a face-on ribbon to bring it edge-on north of that region. This model explains the greater width of the source between the two kinks (see Fig. 10) and also the swift increase in the total intensity (Fig. 12) and Faraday depth north of the major kink, both being due to increased line of sight path length through the emitting region. It might also help in explaining the behavior of the internal filamentation at the major kink. Moreover, the ratio of the width of the Snake south of the major kink to its width north of the major kink is $\sim$3, so only small, smooth variations in the other parameters (electron density and magnetic field strength) are needed to generate the suggested variations in total Faraday depth, rather than large, abrupt changes.

4.2. *A Model of the Snake's Environment*

By combining elements of the three depolarization mechanisms discussed above, it is possible to construct a picture of the Snake and the surrounding medium which explains the observed polarization characteristics. The important points are that (1) the beam depolarization study shows that there is an external Faraday rotating medium with clumpy structure on scales of 5″–10″; (2) the bandwidth depolarization study indicates that rotation measures at least as high as 5500 rad m^{-2} are generated by this medium, with an increasing trend toward the Galactic plane; and (3) internal depolarization causes a fall-off in observable polarization north of the major kink, independent of the influence of the external screen.

Given that the scale size of turbulent cells in the disk of the Galaxy appears to be 10–100 pc (Ohno & Shibata 1993), the small size of the cells found here suggests that the Faraday screen might lie in the hot, dense disturbed medium in the Galactic center, at which distance they must be 0.2–0.4 pc in size. The small-scale variations in rotation measure of 400 rad m^{-2} implied by the clumpiness of the polarized intensity represents 7%–20% of the total rotation measure, and thus require intercell variations of that magnitude in line-of-sight magnetic field strength and/or thermal electron density. The absolute amplitude of these fluctuations must be greater in this screen that in the Galaxy as a whole—also consistent with a Galactic center origin—since the properties found in the disk (B = 4–6 μG and n_e = 0.07–0.2 cm^{-3}; Ohno & Shibata 1993) would give rise to the observed rotation measure variations over paths of 50–100 pc, many times larger than the cell size found here.

The spatial extent of this medium can be further constrained by noting that, like the Snake, the Arc's polarized emission is rapidly depolarized within $\sim$0°.2 of the Galactic plane (see Seiradakis et al. 1985; Haynes et al. 1992), while the adjacent nonthermal source G357.7−0.1 is also strongly polarized but shows no rotation measures in excess of $\sim$1000 rad cm^{-2}, despite its low latitude (Stewart et al. 1994). Low-latitude extragalactic sources elsewhere in the Galaxy ($50° < l < 90°$) also do not display rotation measures larger than this value (Tabara & Inoue 1980; Clegg et al. 1992). This limits the longitude extent of the medium to less than 2° from the Galactic center. This is the same region occupied by the nuclear molecular disk in the Galactic center (see Güsten 1989, and references therein).

4.2.1. *The Nuclear Disk*

The molecular disk in the Galactic center—also referred to as a "diffuse elliptical component" in the infrared observations of Little & Price (1985)—is well displayed in the *IRAS* images

(Gautier et al. 1984) as a strong concentration in the nuclear region, spanning longitudes from ~358°.6 (Sgr E) through to ~1°.2 (Sgr D) with a latitude range of ±0°.25–0°.5 (Cox & Laureijs 1989). Longitude and latitude profiles of the *IRAS* HCON3 images of this region are shown in Figure 16. A corresponding latitude profile was made from the 8750 MHz ($\lambda = 3.5$ cm) Parkes total intensity data of Haynes et al. (1992). The zero level of these radio data is unknown since they were only measured in the range $-1°.2 < b < +1°.1$, so the radio intensities have been offset in amplitude by 0.1 Jy beam^{-1} and multiplied by 2.15×10^9 beam sr^{-1} to give a good numerical agreement for both the peak and tails of the two intensity distributions. The result is plotted in Figure 16*b*. Note the excellent overall agreement between the radio and infrared profiles (the deviations at negative latitudes are due to nonthermal emission from SNRs G359.1−0.5 and G359.0−0.9; see Fig. 1), suggesting that the radio emission is substantially thermal in origin (Broadbent, Haslam, & Osbourne 1989).

By considering the measured intensity of the background radiation at several frequencies between 408 MHz (Little 1974) and 10 GHz (Handa et al. 1987), it is concluded that indeed

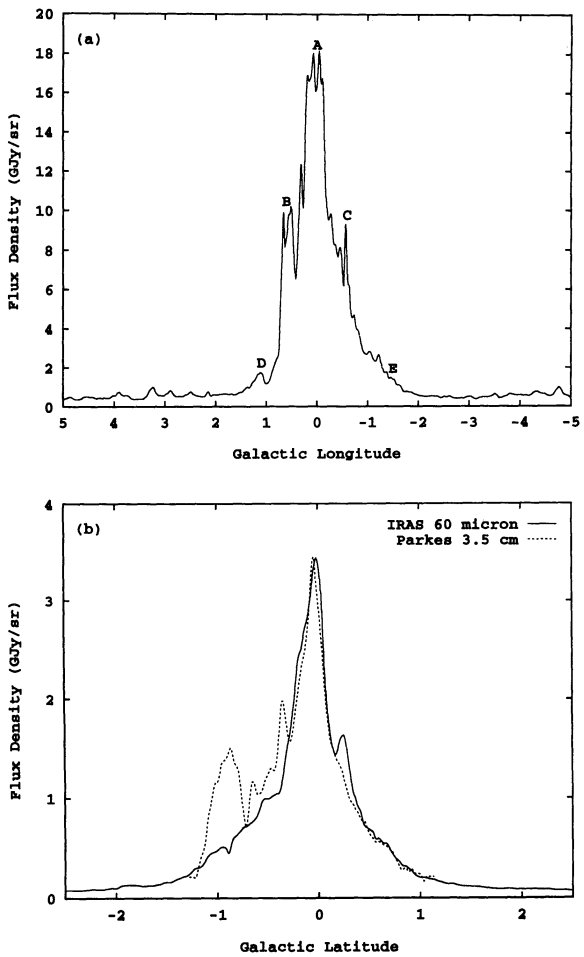

FIG. 16.—Profiles in (*a*) longitude and (*b*) latitude of the 60 μm (*IRAS*) emission, showing the nuclear component. The letters in (*a*) refer to the named source complexes, Sgr A–E. The profile in (*b*) was taken at the longitude of the Snake ($l \simeq 359°.1$), and superimposed on it (*dashed line*) is the corresponding latitude profile from Parkes 8750 MHz data, offset and rescaled to bring the profiles into agreement for display purposes (see text for details).

probably somewhat less than half of the observed radio emission at 8750 MHz is attributable to nonthermal processes. Converting the observed 8750 MHz flux density to brightness temperature gives $T_b = 1$ K, and adopting an upper limit of 50% nonthermal emission yields a thermal brightness temperature in the range $\gtrsim 0.5$–1 K. The further assumption of a thermal electron temperature of $T_e \simeq 10^4$ K results in a derived free-free optical depth of $\tau \simeq 0.5$–1×10^{-4} and an emission measure of $E_M \simeq 0.5$–2×10^4 pc cm^{-6}. For a path length of $L \simeq 100$ pc, this emission measure requires a thermal electron density of $n_e \simeq 7$–14 cm^{-3}, consistent with the value derived above to account for the apparent internal depolarization. Note that this is the density of *ionized* gas; for comparison, the molecular (H_2) clouds in the disk have a mean density of 10^4 cm^{-3} with a volume-averaged density of $\sim 10^2$ cm^{-3} in the inner 500 pc (Güsten 1989). In fact, the region under consideration here is about half of that radius and contains the most dense regions, so the volume-averaged density may be up to an order of magnitude higher, implying a mean ionized fraction of up to 1%. An alternative model in which the Faraday rotating medium is arranged in a sheath around the Snake with $L \sim 1$ pc may be ruled out since the electron density required is of order 10^2 cm^{-3}. Aside from requiring a high ionized fraction, such gas would have significant free-free optical depth at low frequencies, in conflict with the observed emission at 330 MHz (Anantharamaiah et al. 1991).

That the suggested component is responsible for a rotation measure of 5.5×10^3 rad m^{-2} further requires that the mean parameters satisfy $n_e B_{\|} L \simeq 6800$ pc cm^{-3} G. For L and n_e as above, the mean line-of-sight magnetic field strength external to the Snake is thus $B_{\|} \simeq 7$ μG. This is in good agreement with the magnetic field strength in the inner Galaxy suggested by Rand & Lyne (1994). The parameters required to explain the observed properties of the Snake therefore do not require any exceptional properties of the nuclear disk environment. The presence of such a magneto-ionic component is also consistent with the large-scale polarimetry work by Tsuboi et al. (1986) and Haynes et al. (1992). This component is not, however, incorporated into models of the Galactic electron density distribution derived from pulsar observations (Cordes et al. 1991; Taylor & Cordes 1993), since no pulsars are known within its boundaries (see Taylor, Manchester, & Lyne 1993). Its very presence might itself partly account for this: adjacent pulsars at distances comparable to the Galactic center have dispersion measures of ~600 pc cm^{-3} (see Taylor, Manchester, & Lyne 1993, and references therein). Any pulsars within or beyond the proposed nuclear component would suffer a further 10^3 pc cm^{-3} or more of dispersion measure. This could hinder the detection of pulsars in this small region of the sky, although Johnston (1994) claims that even dispersion measures of many thousands would no prove troublesome and presents a model in which the population of pulsars in the inner Galaxy is small. Nonetheless, a concentrated search for high-dispersion pulsars in this region might prove fruitful and also assist in verifying the properties of the component derived here.

5. CONCLUSIONS

The detailed imaging and polarimetry campaign undertaken in the study of the Snake has revealed the morphology and environment of this object in some detail, but the secret of this formation and illumination remains unclear. Its physical characteristics—90 μG magnetic field and nonthermal spectrum, for example—agree closely with those found for other

thread- or filament-like objects, and its internal structure is reminiscent of that seen in the Arc feature near Sgr A and G359.54+0.18. However, its location below the Galactic plane and outside the Galactic center lobe places it in a unique environment for these structures and may rule out at least one model of the activity in the Galactic center. Other models considered in this paper—including a jet or ejectum from a supernova event, a star trail or wake, shock fronts, and cosmic strings—are constrained by observational limits on proper motion and variability, but as yet none can be ruled out conclusively on those grounds alone. The presence of kinks in the Snake's structure, however, does place constraints on the types of models which are viable, since few of the models discussed here provide obvious mechanisms for the productions of the kinks. For this reason the electrodynamic models (Benford 1988; Heyvaerts, Norman, & Pudritz 1988) are favored as the most likely to be applicable, since they do allow for nonlinear structures. The kinks also provide further difficulty in the interpretation of the Snake, since no other similar structures (the Arc, the "threads") display such kinks, despite considerable similarities in the other measured properties. The kinks also seem to have some effect on the intensity and spectrum of the emission from the Snake, for reasons which are not yet understood, and it cannot be ruled out that the presence of some object at the most prominent kink is responsible for the illumination of the Snake. Understanding the kinks may this provide great insight into the formation of the Snake and hence also into the other filaments in this region.

The polarimetry performed on the Snake confirms some of its suspected properties, showing through the detection of strong polarization that the emission is nonthermal and that the magnetic field is probably oriented parallel to its long axis. The strong depolarization found allows us to probe the medium along the line of sight to the Snake, providing evidence for a localized magneto-ionic medium in the Galactic nucleus distributed in a disk with a radius of $\sim$250 pc and a thickness of $\sim$60 pc, probably associated with the nuclear molecular disk. The properties indicated for this component are a line-of-sight magnetic field of 7 μG and an electron density of 10 cm^{-3}, consistent with other research. Density and/or magnetic field fluctuations of up to 10% on scales of $\sim$0.5 pc are needed to explain the clumpiness of the observed polarization. The rotation measure generated along paths of length 100 pc through such a region is 5×10^3 rad cm^{-2} with a dispersion measure of 10^3 pc cm^{-3}. This might limit detectability of pulsars on sight lines through this component of the Galaxy, perhaps providing some explanation of the lack of pulsars found there.

Since the two known examples of high rotation measure on which this model is based both occur in filamentary objects in the Galactic center, the question may also be raised as to whether this behavior is intrinsic to this type of object (or the conditions necessary to form the objects). To confirm the wide distribution of the component discussed above, polarised sources and pulsars behind or within it must be found and studied. A further check would be to seek hydrogen recombination lines (recall that the derived emission measure is 10^4 pc cm^{-6}) at low frequencies where the more prominent H II regions are optically thick and contribute little to the observed spectrum (K. R. Anantharamaiah, private communication). It is not clear whether the gas will be smoothly distributed or clumpy: if it is the former, then interferometric observations may not detect the recombination lines. However, the poor directionality of single-dish telescopes at low frequencies will make it difficult to determine if the correct component is being measured.

One of us (A. D. G.) acknowledges receipt of an Australian Postgraduate Research Award during the course of this work. We also thank our referee for his comments. The Molonglo Observatory Synthesis Telescope is operated by the School of Physics with funds from the Australian Research Council and the Science Foundation for Physics within the University of Sydney.

REFERENCES

Alfvén, H. 1942, Nature, 150, 405
Anantharamaiah, K. R., & Pedlar, A. 1990, in Proc. IAU Symp. 140, Galactic and Intergalactic Magnetic Fields, ed. R. Beck, P. P. Kronberg, & R. Wielebinski (Dordrecht: Kluwer), 375
Anantharamaiah, K. R., Pedlar, A., Ekers, R. D., & Goss, W. M. 1991, MNRAS, 249, 262
Australia Telescope. 1992, J. Elec. Electron. Eng. Australia, 12, 103
Backer, D. C., ed. 1987, AIP Conf. Proc. 155, The Galactic Center (New York: AIP)
Bally, J., Stark, A. A., Wilson, R. W., & Henkel, C. 1988, ApJ, 324, 223
Bally, J., & Yusef-Zadeh, F. 1989, ApJ, 336, 173
Bally, J., Yusef-Zadeh, F., & Hollis, J. M. 1989, in Proc. IAU Symp. 136, The Center of the Galaxy, ed. M. Morris (Dordrecht: Kluwer), 189
Benford, G. 1988, ApJ, 333, 735
Blandford, R. D., Kennel, C. F., McKee, C. F., & Ostriker, J. P. 1983, Nature, 301, 586
Blitz, L., Binney, J., Lo, K. Y., Bally, J., & Ho, P. T. P. 1993, Nature, 361, 417
Bridle, A. H., & Schwab, F. R. 1989, in ASP Conf. Proc., Vol. 6, Synthesis Imaging in Radio Astronomy, ed. R. A. Perley, F. R. Schwab, & A. H. Bridle (San Francisco: ASP), 247
Broadbent, A., Haslam, C. G. T., & Osbourne, J. L. 1989, MNRAS, 237, 381
Brown, R. L., & Liszt, H. S. 1984, ARA&A, 22, 223
Burn, B. J. 1966, MNRAS, 133, 67
Caswell, J. L., Haynes, R. F. 1987, A&A, 171, 261
Caswell, J. L., Kesteven, M. J., Bedding, T. R., & Turtle, A. J. 1989, Proc. Astron. Soc. Australia, 8, 184
Caswell, J. L., Kesteven, M. J., Komesaroff, M. M., Haynes, R. F., Milne, D. K., Stewart, R. T., & Willson, S. G. 1987, MNRAS, 225, 329
Chudnovsky, E. M., Field, G. B., Spergel, D. N., & Vilenkin, A. 1986, Phys. Rev. D, 34, 944
Clegg, A. W., Cordes, J. M., Simonetti, J. H., & Kulkarni, S. R. 1992, ApJ, 386, 143
Cordes, J. M., Weisberg, J. M., Frail, D. A., Spangler, S. R., & Ryan, M. 1991, Nature, 354, 121
Cornwell, T. 1989, in ASP Conf. Ser., Vol. 6, Synthesis Imaging in Radio Astronomy, ed. R. A. Perley, F. R. Schwab, & A. H. Bridle (San Francisco: ASP), 277
Cox, P., & Laureijs, R. 1989, in Proc. IAU Symp. 136, The Center of the Galaxy, ed. M. Morris (Dordrecht: Kluwer), 121
Cox, C. I., Gull, S. F., & Green, D. A. 1991, MNRAS, 250, 750
Downes, D., Godd, W. M., Schwarz, U. J., & Wouterloot, J. G. A. 1978, A&AS, 35, 1
Dreher, J. W., Carilli, C. L., & Perley, R. A. 1987, ApJ, 316, 611
Ekers, R. D., van Gorkom, J. H., Schwarz, U. J., & Goss, W. M. 1983, A&A, 122, 143
Gardner, F. F., & Whiteoak, J. B. 1966, ARA&A, 4, 245
Gautier, T. N., et al. 1984, ApJ, 278, L57
Genzel, R., & Townes, C. H. 1987, ARA&A, 25, 377
Gray, A. D. 1994a, MNRAS, 270, 822 (Paper I)
———. 1994b, MNRAS, 270, 835 (Paper II)
———. 1994c, MNRAS, 270, 847
———. 1994d, MNRAS, 270, 861
Gray, A. D., Cram, L. E., Ekers, R. D., & Goss, W. M. 1991, Nature, 353, 237
Gray, A. D., Whiteoak, J. B. Z., Cram, L. E., & Goss, W. M. 1993, MNRAS, 264, 678
Greisen, E. W., & Junor, W. ed. 1990, AIPS Cookbook (Charlottesville: NRAO)
Güsten, R. 1989, in Proc. IAU Symp. 136, The Center of the Galaxy, ed. M. Morris (Dordrecht: Kluwer), 89
Handa, T., Sofue, Y., Nakai, N., Hirabayashi, H., & Inoue, M. 1987, PASJ, 39, 709
Haynes, R. F., Stewart, R. T., Gray, A. D., Reich, W., Reich, P., & Mebold, U. 1992, A&A, 264, 500
Helfand, D. J., & Becker, R. H. 1985, Nature, 313, 117

Heyvaerts, J., Norman, C., & Pudritz, R. E. 1988, ApJ, 330, 718
Insertis, F. M., & Rees, M. J. 1991, MNRAS, 252, 82
Inoue, M., Fomalont, E., Tsuboi, M., Yusef-Zadeh, F., Morris, M., Tabara, H., & Kato, T. 1989, in Proc. IAU Symp. 136, The Center of the Galaxy, ed. M. Morris (Dordrecht: Kluwer), 269
Johnston, S. 1994, MNRAS, 268, 595
Kerr, F. J., & Lynden-Bell, D. 1986, MNRAS, 221, 1023
Kesteven, M. J., Caswell, J. L., Roger, R. S., Milne, D. K., Haynes, R. F., & Wellington, K. J. 1987, Australian J. Phys., 40, 855
Killeen, N. E. B. 1992, AT Manual, Analysis of Australia Telescope Compact Array Data
Killeen, N. E. B., Bicknell, G. V., & Ekers, R. D. 1986, ApJ, 302, 306
Liszt, H. S. 1985, ApJ, 293, L65
———. 1988, in Galactic and Extragalactic Radioastronomy, ed. G. L. Verschuur & K. I. Kellermann (2d ed.; New York: Springer), 359
———. 1992, ApJS, 82, 495
Little, A. G. 1974, in Proc. IAU Symp. 60, Galactic Radio Astronomy, ed. F. J. Kerr & S. C. Simonson (Dordrecht: Reidel), 491
Little, S. J., & Price, S. D. 1985, AJ, 90, 1812
Manka, R., & Bednárek, L. 1991, Ap&SS, 176, 325
McGee, R. X., & Boulton, J. G. 1954, Nature, 173, 985
Mills, B. Y. 1981, Proc. Astron. Soc. Australia, 4, 156
Mirabel, I. F., Rodríguez, L. F., Cordier, B., Paul, J., & Lebrun, F. 1992, Nature, 358, 215
Morris, M., ed. 1989, Proc. IAU Symp. 136, The Center of the Galaxy (Dordrecht: Kluwer)
———. 1990, in Proc. IAU Symp. 140, Galactic and Intergalactic Magnetic Fields, ed. R. Beck, P. P. Kronberg & R. Wielebinski (Dordrecht: Kluwer), 361
Morris, M., & Yusef-Zadeh, F. 1985, AJ, 90, 2511
Napier, P. J., Thompson, R., & Ekers, R. D. 1983, Proc. IEEE, 11, 1295
Nicholls J., & Gray, A. D. 1993, Proc. Astron. Soc. Australia, 10, 223
Nicholls, J., & Le Strange, E. T. 1995, ApJ, 443, 638
Odenwald, S. F. 1989, in Proc. IAU Symp. 136, The Center of the Galaxy, ed. M. Morris (Dordrecht: Kluwer), 205
Odenwald, S. F., & Fazio, G. G. 1984, ApJ, 283, 601
Ohno, H., & Shibata, S. 1993, MNRAS, 262, 953
Oort, J. H. 1977, ARA&A, 15, 295
Pedlar, A., Anantharamaiah, K. R., Ekers, R. D., Goss, W. M., van Gorkom, J. H., Schwarz, U. J., & Zhao, J.-H. 1989, ApJ, 342, 769
Rand, R. J., & Lyne, A. G. 1994, MNRAS, 268, 497
Reich, W. 1989, in Proc. IAU Symp. 136, The Center of the Galaxy, ed. M. Morris (Dordrecht: Kluwer), 265
Reich, W., & Fürst, E. 1984, A&AS, 57, 165
Reich, W., Fürst, E., Reich, P., & Junkes, N. 1988, in Proc. IAU Colloq. 101, Supernova Remnants and the Interstellar Medium, ed. R. S. Roger & T. L. Landecker (Cambridge: Cambridge Univ. Press), 293
Reich, W., Fürst, E., Reich, P., & Reif, K. 1990, A&AS, 85, 633
Reich, W., & Schlickeiser, R. 1992, A&A, 256, 408
Robertson, J. G. 1991, Australian J. Phys., 44, 729
Sanders, R. H. 1989, in Proc. IAU Symp. 136, The Center of the Galaxy, ed. M. Morris (Dprdrecht: Kluwer), 77
Sault, R. J., & Killeen, N. E. B. 1992, MIRIAD Users' Guide
Seiradakis, J. H., Lasenby, A. N., Yusef-Zadeh, F., Wielebinski, R., & Klein, U. 1985, Nature, 317, 697
Shaver, P. A., Salter, C. J., Patnaik, A. R., van Gorkom, J. H., & Hunt, G. C. 1985b, Nature, 313, 113
Sofue, Y., & Handa, T. 1984, Nature, 310, 568
Stewart, R. T., Haynes, R. F., Gray, A. D., & Reich, W. 1994, ApJ, 432, L39
Tabara, H., & Inoue, M. 1980, A&AS, 39, 379
Taylor, J. H., & Cordes, J. M. 1993, ApJ, 411, 674
Taylor, J. H., & Manchester, R. N., & Lyne, A. G. 1993, ApJS, 88, 529
Thompson, A. R., Moran, J. M., & Swenson, G. W., Jr. 1986, Interferometry and Synthesis in Radioastronomy (New York: Wiley), 97ff
Tsuboi, M., Ionue, M., Handa, T., Tabara, H., Kato, T., Sofue, Y., & Kaifu, N. 1986, AJ, 92, 818
Uchida, K. I., Morris, M., Bally, J., Pound, M., & Yusef-Zadeh, F. 1992, ApJ, 398, 128
Uchida, K. I., Morris, M., & Yusef-Zadeh, F. 1992, AJ, 104, 1533
Vilenkin, A. 1988, Nature, 332, 610
Vilenkin, A., & Field, G. B. 1987, Nature, 326, 772
Whiteoak, J. B. Z., & Green, A. J. 1995, in preparation
Whiteoak, J. B. Z., Large, M. I., Cram, L. E., & Piestrzynski, B. 1989, Proc. Astron. Soc. Australia, 8, 176
Yusef-Zadeh,F. 1986, Ph.D. thesis, Columbia Univ.
Yusef-Zadeh, F., & Bally, J. 1987, Nature, 330, 455
———. 1989, in Proc. IAU Symp. 136, The Center of the Galaxy, ed. M. Morris (Dordrecht: Kluwer), 197
Yusef-Zadeh, F., & Morris, M. 1987a, ApJ, 320, 545
———. 1987b, ApJ, 322, 721
———. 1987c, AJ, 94, 1178
Yusef-Zadeh, F., Morris, M., & Chance, S. 1984, Nature, 310, 557
Yusef-Zadeh, F., Morris, M., Lasenby, A. N., Seiradakis, J. H., & Wielebinski, R. 1990, in Proc. IAU Symp. 140, Galactic and Intergalactic Magnetic Fields, ed. R. Beck et al. (Dordrecht: Kluwer), 373